


# Relationship Between the Diode Ideality Factor and the Carrier Recombination Resistance in Organic Solar Cells

Leiping Duan, Haimang Yi, Cheng Xu, Mushfika Baishakhi Upama, Md Arafat Mahmud, Dian Wang, Faiazul Haque Shabab, and Ashraf Uddin 

**Abstract**—Organic solar cells are about to become a potential competitor to silicon solar cells. It is vital to understand the carrier recombination mechanism of organic solar cells to improve the device performance further. The diode ideality factor and carrier recombination resistance are the two commonly used parameters to describe the nongeminate, also called trap-assisted, recombination in solar cells. Herein, we demonstrated the relationship between these two parameters and derived an equation that can be used as a new method to estimate the carrier recombination resistance in organic solar cells. PBDB-T:ITIC-based nonfullerene organic solar cells, and PTB7:PC<sub>71</sub>BM and PffBT4T-2OD:PC<sub>71</sub>BM-based fullerene organic solar cells were fabricated to provide experimental proofs for our demonstration. A comparative study has been done between the fresh and aged PBDB-T:ITIC-based devices to further analyze the relationship between the carrier recombination resistance and the diode ideality factor.

**Index Terms**—Carrier recombination resistance, diode ideality factor, nonfullerene acceptor, organic solar cells.

## I. INTRODUCTION

**S**OLUTION-PROCESSED bulk heterojunction (BHJ) organic solar cells with advantages of low weight, flexibility, semitransparency, and short energy payback time have attracted much research attention in past few decades [1]–[3]. The power conversion efficiency (PCE) of solution-processed organic solar cells has reached 14.62% to date [4], [5]. Many researchers found that the nongeminate recombination of carriers in BHJ is the main reason that limited the performance of the solar cell. Therefore, the understanding of the mechanism behind the carrier recombination becomes very crucial. It is believed that reducing the nongeminate recombination can further increase

the PCE of solution-processed BHJ organic solar cells [6]–[13]. The diode ideality factor is a useful tool for the investigation that can indicate the effects of traps on carrier recombination in the photovoltaic device [14]–[17].

In 1952, Shockley and Read [18] first reported a method with ideal diode solar cell current–voltage equation and single-exponential diode model to analyze the performance of solar cells. The ideal solar cell current–voltage equation is listed as follows:

$$J = J_L - J_0(e^{(qV/nKT)} - 1) \quad (1)$$

where  $J_L$  is the light current density,  $J_0$  is the carrier recombination current density (also called saturation current density),  $q$  is the elementary charge,  $V$  is the applied voltage,  $K$  is the Boltzmann constant,  $T$  is the operating temperature in Kelvin scale, and  $n$  is the diode ideality factor.

In this model, the ideal photovoltaic device is assumed to precisely follow the solar cell current–voltage equation and the diode ideality factor  $n$  acts as an indicator that can describe the difference between the ideal device and practical device [18]. Typically, the value of the diode ideality factor ranges from 1 to 2 for real devices. The value of  $n > 1$  indicates that there are traps involved in a carrier recombination mechanism in solar cells. When the value of  $n$  approaches 2, it suggests the midgap states become the dominated component of the recombination in solar cells [16], [19]. Thus, the diode ideality factor is an important parameter that can describe the electrical behavior of photovoltaic devices.

There are various methods to estimate the diode ideality factor based on different theories including single-diode model, forward bias, Suns- $V_{oc}$ , static model, and a single  $I$ – $V$  dataset [20]. In this study, the ideality factor will be determined by using the most common method that is based on the dark current density–voltage ( $J$ – $V$ ) curve [21]. In this method, the parasitic resistances are ignored. The ideal solar cell current–voltage equation in the dark can be written as

$$J_{\text{dark}}(V) = J_0 \left( e^{\frac{qV_a}{nKT}} - 1 \right) \quad (2)$$

where  $J_{\text{dark}}$  is the dark current density,  $J_0$  is the carrier recombination current density, and  $V_a$  is the applied bias voltage. By using the  $J$ – $V$  characteristics in the dark, the diode ideality factor  $n$  can be calculated from the slope in the exponential

Manuscript received June 5, 2018; revised July 26, 2018; accepted September 12, 2018. This work was supported by the Australian Government Research Training Program Scholarship. (Corresponding authors: Leiping Duan; Ashraf Uddin.)

The authors are with the School of Photovoltaic and Renewable Energy Engineering, University of New South Wales, Sydney, N.S.W. 2052, Australia (e-mail: leiping.duan@student.unsw.edu.au; haimang.yi@student.unsw.edu.au; z5084835@student.unsw.edu.au; m.upama@unsw.edu.au; mdarafat.mahmud@unsw.edu.au; dian.wang@student.unsw.edu.au; f.haque@student.unsw.edu.au; a.uddin@unsw.edu.au).

This paper has supplementary downloadable material available at <http://ieeexplore.ieee.org>.

Color versions of one or more of the figures in this paper are available online at <http://ieeexplore.ieee.org>.

Digital Object Identifier 10.1109/JPHOTOV.2018.2870722

region of the curve. The diode ideality factor extracted from the  $J$ - $V$  curve can be represented as follows [22]:

$$n = \frac{q}{KT} \frac{dV_a}{d \ln(J_{\text{dark}})}. \quad (3)$$

On the other hand, carrier recombination resistance ( $R_{\text{rec}}$ ) is another electrical parameter of solar cells associated with the nongeminate recombination that can be extracted from the impedance measurement. During the impedance measuring, the carrier transport-recombination behavior of solar cells will produce a transmission line (TL). By fitting the TL to the TL pattern, the carrier transport resistance  $R_{\text{tr}}$  and recombination resistance  $R_{\text{rec}}$  can be figured out.  $R_{\text{rec}}$  ( $\Omega$ ) is related to the carrier recombination in the solar cell and can be represented as [23], [24]

$$R_{\text{rec}} = \frac{1}{A} \left( \frac{\partial J_{\text{rec}}}{\partial V_e} \right)^{-1} \quad (4)$$

where  $J_{\text{rec}}$  is the recombination current density under effective measuring voltage  $V_e$ .

Electrical impedance spectroscopy (EIS) is a widely applied method for impedance measurements. It mainly focuses on obtaining the electrical response of the device to get the impedance information under an applied electrical small signal in a frequency scale [25]. By using different models with the impedance measurements, various processes can be interpreted as conducting polymers and semiconductors. [26]. EIS is also a widely used method to extract the carrier recombination resistance for organic photovoltaic devices.

In this work, the relationship between the diode ideality factor  $n$  and the carrier recombination resistance  $R_{\text{rec}}$  is investigated, and a relation equation between these two parameters is derived. Experimentally, we fabricated three different types of organic solar cells based on the polymer donor material, poly[(2,6-(4,8-bis(5-(2-ethylhexyl)thiophen-2-yl)-benzo[1,2-b:4,5-b']dithiophene))-alt-(5,5-(1',3'-di-2-thienyl-5',7'-bis(2-ethylhexyl) benzo [1', 2'-c:4',5'-c']dithiophene-4,8-dione))] (PBDB-T) with nonfullerene acceptor material, 3,9-bis(2-methylene-(3-(1,1-dicyanomethylene)-indanone))-5, 5, 11, 11-tetrakis(4-hexylphenyl)-dithieno[2,3-d:2',3'-d']-s-indaceno[1,2-b:5,6-b']dithiophene (ITIC), the polymer donor material poly({4,8-bis[(2-ethylhexyl)oxy]benzo[1,2-b:4,5-b']dithiophene-2,6-diyl}{3-fluoro-2-[(2-ethylhexyl)carbonyl]thieno[3,4-b]thiophenediyl}) (PTB7) with fullerene acceptor material [6,6]-phenyl C71 butyric acid methyl ester (PC<sub>71</sub>BM), and the polymer donor material poly[(5,6-difluoro-2,1,3-benzothiadiazol-4,7-diyl)-alt-(3,3''-di(2-octyldodecyl)-2,2',5',2'',5'',2'''-quaterthiophen-5,5'''-diyl)] (PffBT4T-2OD) with fullerene acceptor material PC<sub>71</sub>BM. Moreover, a comparative study between the fresh and aged PBDB-T:ITIC-based solar cells has been conducted. Known from the current density-voltage ( $J$ - $V$ ) measurement, the fresh PBDB-T:ITIC-based device with an inverted structure of ITO/ZnO/active layer/MoO<sub>3</sub>/Ag exhibits the average PCE of 10.8% with the ideality factor around 1.60, while the aged PBDB-T:ITIC-based device exhibits the degraded average PCE of 9.16% with the ideality factor increased to around 1.88. The

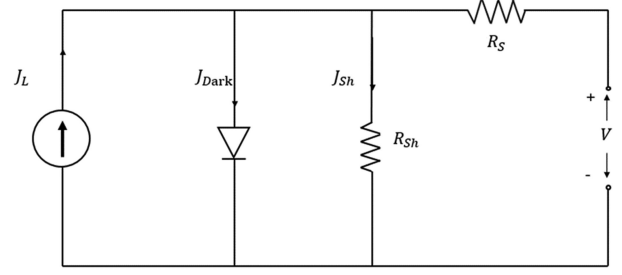


Fig. 1. Solar cell equivalent circuit with consideration of series resistance and shunt resistance.

PTB7:PC<sub>71</sub>BM and PffBT4T-2OD:PC<sub>71</sub>BM-based devices, fabricated in the same device structure, show the average PCE of 6.07% and 7.87%, respectively. The diode ideality factor for PTB7:PC<sub>71</sub>BM devices and PffBT4T-2OD:PC<sub>71</sub>BM devices is around 1.79 and 1.64, respectively. This work reported a new method to calculate the carrier recombination resistance by using the derived relation equation with the diode ideality factor extracted from the experimental devices. The carrier recombination resistance calculated by using the relation equation for the fresh PBDB-T:ITIC device, the aged PBDB-T:ITIC device, the PTB7:PC<sub>71</sub>BM device, and PffBT4T-2OD:PC<sub>71</sub>BM device are 241.02, 186.38, 287.95, and 887.69  $\Omega \cdot \text{cm}^2$ , respectively. A comparison is made between the calculated the carrier recombination resistance and the carrier recombination resistance extracted from the EIS. The results further demonstrated the relationship between the diode ideality factor and the carrier recombination resistance as well as the validity of the derived relation equation.

## II. THEORETICAL ANALYSIS

From a fabricated solar cell, there are several parameters that can be directly measured from the  $J$ - $V$  test including short-circuit current ( $J_{\text{sc}}$ ), open-circuit voltage ( $V_{\text{oc}}$ ), fill factor (FF), and PCE. With the consideration of the series resistance ( $R_s$ ) and shunt resistance ( $R_{\text{sh}}$ ), the equivalent circuit of a solar cell can be drawn as in Fig. 1, and the ideal solar cell current-voltage equation (1) can be modified to [27]

$$J = J_L - J_0 \left( e^{\frac{q(V + JR_s)}{nKT}} - 1 \right) - \frac{V + JR_s}{R_{\text{sh}}}. \quad (5)$$

By using the above-mentioned measurable parameters and ideal diode equation (5), we can derive an analytical expression of the diode ideality factor.

If the solar cell is at the short-circuit condition ( $V = 0$ ) and the simulated one sun illumination test condition (AM1.5, 100 mW/cm<sup>2</sup>), (1) can be rewritten as follows.

When applied bias voltage  $V = 0$ ,  $T = T_{\text{STC}}$ , then from (1):

$$J = J_L - J_0 = J_{\text{sc}} \quad (6)$$

where  $T_{\text{STC}}$  is the temperature under the standard test condition, which is 298 K (25 °C).

If  $J_0$  is negligible, when applying the assumptions (6) to the ideal diode equation (1), the equation can be rewritten as

$$J_{sc} \approx J_L. \quad (7)$$

If the solar cell is at an open-circuit condition ( $J = 0$ ) and the simulated one sun test condition (AM1.5, 100 mW/cm<sup>2</sup>), (1) can be rewritten as

$$V = V_{oc} \quad (8)$$

where  $V_{oc}$  is the open-circuit voltage under the standard test condition, (1) can be written as

$$0 = J_L - J_0 \left( e^{\frac{qV_{oc}}{nKT}} - 1 \right). \quad (9)$$

Substituting (7) into (9), the equation can be rewritten as

$$J_{sc} = J_0 \left( e^{\frac{qV_{oc}}{nKT}} - 1 \right). \quad (10)$$

Finally, the analytical expression of the diode ideality factor can be derived from (10) as follows:

$$n = \frac{qV_{oc}}{KT \left( \ln \frac{J_{sc}}{J_0} + 1 \right)}. \quad (11)$$

It is worth to mention that, for the above-mentioned derivation, since the shunt resistance is usually much larger than the series resistance, the  $\frac{V+JR_s}{R_{sh}}$  term is assumed to be ignored [27]. Known that the carrier recombination resistance ( $R_{rec}$ ) can be represented by the effect voltage, device area, and the recombination current density in (4) [23], [24], [28], (4) can be rewritten to express  $R_{rec}$  ( $\Omega$  cm<sup>2</sup>) with the carrier recombination current density as follows:

$$R_{rec} = \frac{V_e}{J_{rec}} \quad (12)$$

where  $J_{rec}$  is the carrier recombination current density.

Thus, the carrier recombination current density can be expressed with recombination resistance  $R_{rec}$  as

$$J_{rec} = \frac{V_e}{R_{rec}}. \quad (13)$$

In the ideal diode model, the recombination current can be expressed as [29]

$$J_{rec} = J_0 \left( e^{\frac{q(V+JR_s)}{nKT}} - 1 \right). \quad (14)$$

Substituting (13) into (14),  $J_0$  can be expressed as

$$J_0 = \frac{R_{rec}}{V_e} \left( e^{\frac{q(V+JR_s)}{nKT}} - 1 \right)^{-1}. \quad (15)$$

Substituting (15) into (11), the relationship between the diode ideality factor and the carrier recombination resistance can be written as follows:

$$R_{rec} = \frac{V_e}{J_{sc}} \left( e^{\frac{q(V_{oc}-V_e-B)}{nKT}} \right) \quad (16)$$

where  $B = JR_s$  represents the voltage loss across the series resistance.

Equation (16) clearly shows the relationship between the carrier recombination resistance and the diode ideality factor, and

it presented a new method to estimate the carrier recombination resistance by using the diode ideality factor.

### III. EXPERIMENTAL RESULTS AND DISCUSSION

In this study, we fabricated BHJ organic solar cells with an inverted structure of ITO/ZnO/PBDB-T:ITIC or PTB7:PC<sub>71</sub>BM or PffBT4T-2OD:PC<sub>71</sub>BM/MoO<sub>3</sub>/Ag [see Fig. 2(a)]. The device fabrication details, as well as characterization details, are given in the Support information. The chemical structures of materials used in this study are shown in Fig. 2(b). The ZnO layer and MoO<sub>3</sub> layer act as electron transport layer and hole transport layer in the device. The fresh PBDB-T:ITIC devices were stored in the glove box filled with N<sub>2</sub> gas for 28 days to become aged devices. To determine the photoelectrical performance, the current density–voltage ( $J$ – $V$ ) curve was measured for both fresh and aged organic solar cells under the simulated one sun test condition (AM1.5, 100 mW/cm<sup>2</sup>). The  $J$ – $V$  curves for PBDB-T:ITIC-based devices are shown in Fig. 3(a) and  $J$ – $V$  curves for PTB7:PC<sub>71</sub>BM and PffBT4T-2OD:PC<sub>71</sub>BM-based devices are shown in Fig. S1(a). The corresponding photovoltaic parameters are listed in Table I.

For the PBDB-T:ITIC-based solar cells, the fresh device demonstrated a high average PCE of 10.79%, while the average PCE of the aged device after stored for 28 days reduced to 9.16%. The series resistance of aged devices was increased from 5.91 to 11.14  $\Omega$  cm<sup>2</sup>. Other parameters including  $V_{oc}$ ,  $J_{sc}$ , FF, and  $R_{sh}$  for aged devices all show reductions in a different degree where the average shunt resistance shows the most significant drop, which decreases by over 50% from 680.8 to 242.8  $\Omega$  cm<sup>2</sup>. For the PTB7:PC<sub>71</sub>BM and PffBT4T-2OD:PC<sub>71</sub>BM-based devices, the average PCE of 6.07% and 7.87%, respectively, has been obtained. Fig. 3(b) displays the dark current density to voltage curve of both fresh and aged PBDB-T:ITIC-based devices. It is obvious to observe that the fresh device has a much lower leakage current when under the reverse bias. The high leakage current indicates the low shunt resistance, which further illustrated the reductions of  $R_{sh}$  for aged devices [30]. The low value of  $R_{sh}$  also indicates the higher charge carrier recombination in the device [31]. The small dark leakage current of the fresh device is also responsible for its higher  $V_{oc}$  value since the  $V_{oc}$  value can be directly estimated by using the short-circuit current density and the dark saturation current density following the ideal diode model with (10) [32]. Moreover, the series resistance of the device can be extracted from the dark  $J$ – $V$  curve. The steeper the slope at a high voltage range ( $>0.75$  V), the lower the series resistance [33]. The fresh device and aged device exhibit very similar slope on the dark  $J$ – $V$  curve at a high voltage range  $>0.75$  V, which indicates there is no significant difference in the series resistance value between the fresh and aged device. The degradation of aged devices is mainly ascribed to the changes in the fundamental materials as well as the contact effects caused by the influence of the environment [34]. The dark  $J$ – $V$  curves for the PTB7:PC<sub>71</sub>BM and PffBT4T-2OD:PC<sub>71</sub>BM-based devices are shown in Fig. S1(b).

The  $C$ – $V$  measurement was conducted to further investigate the performance difference between the fresh and aged

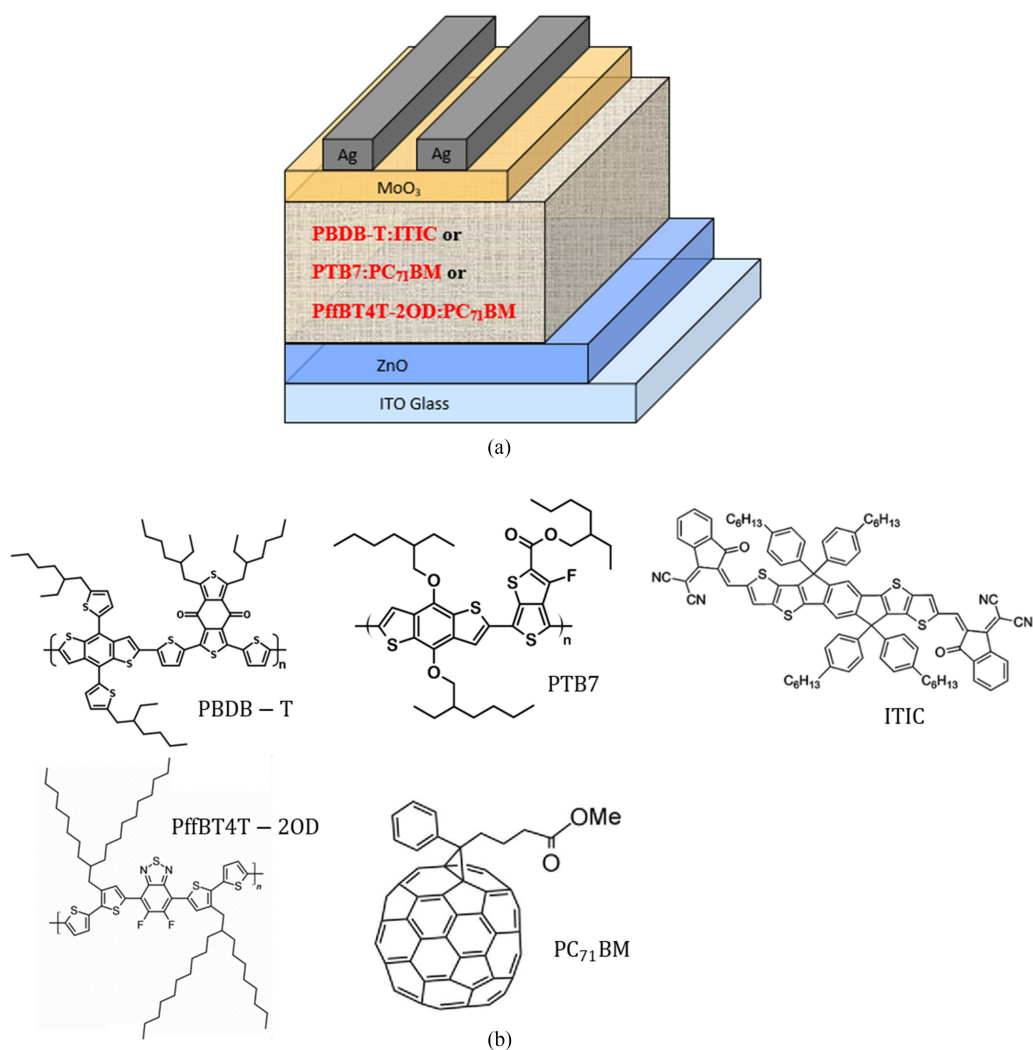


Fig. 2. (a) Schematic diagram of the device structure of organic solar cells. (b) Chemical structures of donor and acceptor materials used.

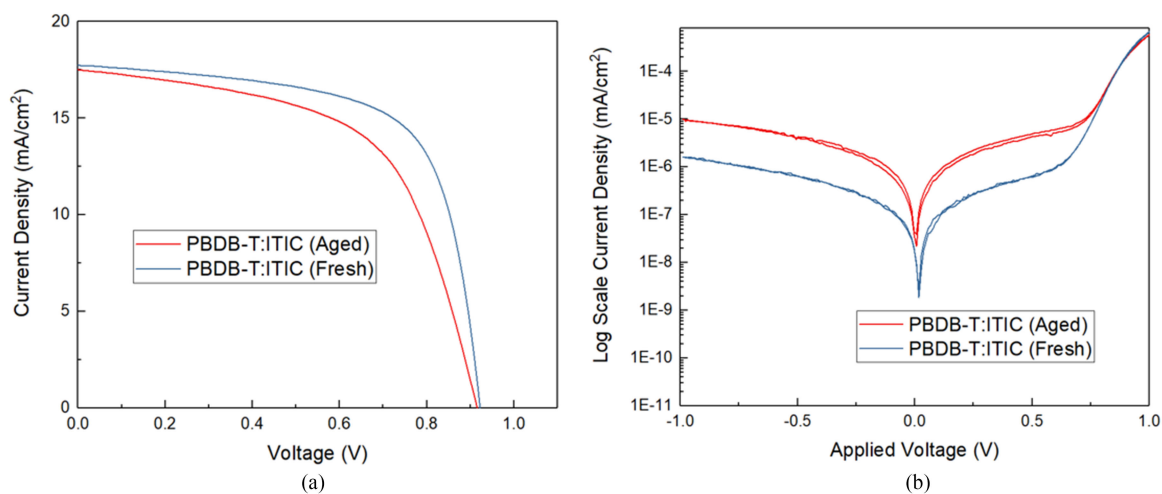


Fig. 3. (a)  $J-V$  curve for fresh and aged PBDB-T:ITIC-based organic solar cells under simulated one sun light at room temperature. (b) Dark  $J-V$  curve for fresh and aged PBDB-T:ITIC-based organic solar cells.



TABLE I  
PHOTOVOLTAIC PERFORMANCE PARAMETERS OF FRESH AND AGED PBDB-T:ITIC-BASED DEVICES, PTB7:PC<sub>71</sub> BM DEVICES, AND  
PFBT4T-2OD:PC<sub>71</sub> BM-BASED DEVICES UNDER SIMULATED ONE SUN LIGHT TEST CONDITION (AM1.5, 100 mW/cm<sup>2</sup>)

| Device                        | $V_{oc}$ (V) | $J_{sc}$ (mA/cm <sup>2</sup> ) | FF (%)      | Ave. PCE (%) | Series Resistance<br>$R_s$ ( $\Omega$ cm <sup>2</sup> ) | Shunt Resistance<br>$R_{sh}$ ( $\Omega$ cm <sup>2</sup> ) |
|-------------------------------|--------------|--------------------------------|-------------|--------------|---|---|
| <b>PBDB-T:ITIC</b><br>(Fresh) | 0.923±0.002  | 17.92±0.03                     | 0.653±0.007 | 10.79±0.02%  | 5.91±0.45   | 680.8±19.6  |
| <b>PBDB-T:ITIC</b><br>(Aged)  | 0.915±0.002  | 17.50±0.09                     | 0.573±0.11  | 9.16±0.13%   | 11.14±1.44  | 242.8±24.0  |
| <b>PTB7:PC71BM</b>            | 0.709±0.002  | 16.87±0.03                     | 0.507±0.003 | 6.07±0.06%   | 9.48±0.06   | 298.8±3.03  |
| <b>PfBT4T-<br/>2OD:PC71BM</b> | 0.775±0.004  | 17.60±0.20                     | 0.577±0.018 | 7.87±0.22%   | 6.63±1.01   | 116.5±22.3  |

The short-circuit current density ( $J_{sc}$ ), open-circuit voltage ( $V_{oc}$ ), fill factor (FF), series resistance ( $R_s$ ), shunt resistance ( $R_{sh}$ ), and power conversion efficiency (PCE) are estimated from the averages of at least five devices.

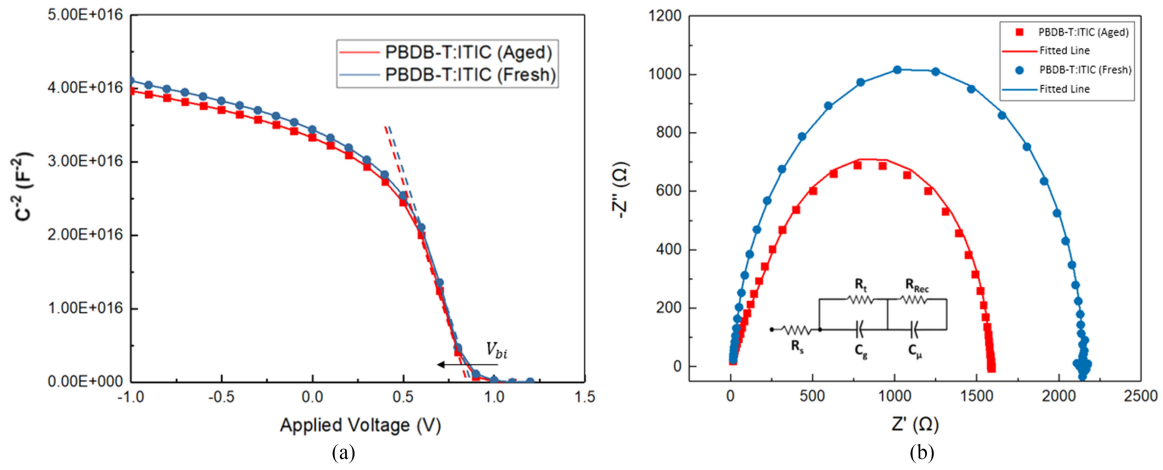


Fig. 4. (a) Mott Schottky curve of the fresh device and the aged device under the dark condition at 10 kHz. (b) Nyquist plot of the fresh and aged PBDB-T:ITIC-based device under the dark condition at 0.8 V voltage bias with the equivalent electrical circuit used for fitting and simulation.

PBDB-T:ITIC-based device. The Mott Schottky curves under 10 kHz representing the relationship between the capacitance and the voltage applied are shown in Fig. 4(a). The built-in potential ( $V_{bi}$ ) of the device can be estimated by extracting the intercept point of the curve with the  $x$ -axis. It can be seen that the aged device has a slightly decreased  $V_{bi}$ , which corresponds to its reduced  $V_{oc}$ . The low  $V_{bi}$  indicates an inefficient operation, since that when the operating voltage is higher than  $V_{bi}$  for a photo device, the net electrical field in the device will reverse, which can restrict the extraction of the charge carriers [35]. The inefficient operation under the adverse electrical field condition for the aged device also explained the lower fill factor when compared with the fresh device.

The EIS study was performed to investigate the conductive electronic characteristics as well as carrier recombination. The EIS study focused on the test of response of the electrical device under an external applied alternating current (ac) signal [36], [37]. For the PBDB-T:ITIC-based devices, the ac impedance test was conducted at the applied voltage of 0.8 V,

and for the PTB7:PC<sub>71</sub> BM and PFBT4T-2OD:PC<sub>71</sub> BM-based devices, the ac impedance test was conducted at the applied voltage of 0.6 V. The applied voltage used for the EIS study was slightly lower than  $V_{oc}$  of devices. This is because, under low voltage bias, the traps are likely to respond to the modulation signal, while the high voltage bias can suppress the influence by the trap state [38]. Fig. 4(b) displays the impedance data in a Nyquist plot for both fresh and aged PBDB-T:ITIC-based devices from 1 Hz frequency to 1 MHz frequency. The equivalent electrical circuit, used for fitting and simulation, is shown in Fig. 4(b), which consists of two series-connected parallel resistance–capacitance ( $RC$ ) components [39]. Since, in the typical Cole–Cole plots, two arcs occur at low-frequency range and high-frequency range, it requires two parallel  $RC$  elements to conduct the simulation. The obtained impedance data exhibit a typical semicircle shape, which can precisely match this parallel  $RC$  equivalent circuit [40]. In the equivalent electrical circuit,  $R_s$  is the series resistance that includes the resistance of each ohmic components and the contact resistance between each layer

TABLE II  
ELECTRICAL PARAMETERS EXTRACTED FROM THE FITTING OF THE NYQUIST PLOT BY USING THE EQUIVALENT CIRCUIT FOR ALL DEVICES

| Name of Parameters             | PBDB-T:ITIC (Fresh) | PBDB-T:ITIC (Aged) | PTB7:PC <sub>71</sub> BM | PffBT4T-2OD:PC <sub>71</sub> BM |
|--------------------------------|---------------------|--------------------|--------------------------|---------------------------------|
| <b>Rs (Ω cm<sup>2</sup>)</b>   | 1.92                | 1.62               | 3.48                     | 2.53                            |
| <b>Rt (Ω cm<sup>2</sup>)</b>   | 7.18                | 14.76              | 47.52                    | 41.52                           |
| <b>Rrec (Ω cm<sup>2</sup>)</b> | 247.20              | 172.80             | 289.20                   | 951.60                          |
| <b>Cg (nF/cm<sup>2</sup>)</b>  | 283.33              | 104.17             | 57.33                    | 493.33                          |
| <b>Cμ (nF/cm<sup>2</sup>)</b>  | 60.58               | 140.00             | 149.16                   | 171.67                          |

[41], [42].  $R_t$  represents the transport resistance that is mainly related to the transportation of the charge carrier.  $R_{rec}$  is interpreted as the carrier recombination resistance that is directly associated with the nongeminate recombination in the device, since it is extracted from the dark condition without photon generations [40].  $C_g$  and  $C_\mu$  are dielectric component capacitance and distributed chemical capacitance, respectively.  $C_g$  acts as an indicator of the dielectric component in the device diode model, and  $C_\mu$  suggests the charge accumulation that cannot be extracted at electrodes [43]. The obtained impedance results of fresh and aged PBDB-T:ITIC-based devices were fitted with this circuit displayed as points and fitting lines in Fig. 4(b). For the PTB7:PC<sub>71</sub>BM and PffBT4T-2OD:PC<sub>71</sub>BM-based device, the Nyquist plot and fitted line are shown in Fig. S2(a). The corresponding parameters from the fitting are presented in Table II.

In Table II, the series resistance of the fresh PBDB-T:ITIC-based device here is almost the same with the aged device, which is coherent with the observation and analysis from the dark  $J$ - $V$  curve. It is worth to mention that the series resistance  $R_s$  extracted from the EIS and the dark  $J$ - $V$  curve is different than that extracted from the  $J$ - $V$  curve under illumination since measurements for EIS and dark  $J$ - $V$  are conducted under the dark condition, the actual current flow in devices during the measurement is reverse to the current under the illuminated operating condition. On the other hand, the fresh PBDB-T:ITIC-based device exhibits a 38% higher carrier recombination resistance, which indicates less nongeminate recombination in the device. By using the value of transport resistance  $R_t$  and the distributed chemical capacitance  $C_\mu$ , the related electron diffusion time as well as the electron diffusivity  $D_n$  can be calculated by using the following equations [40]:

$$\tau_d = R_t \times C_\mu \quad (17)$$

$$D_n = \frac{L^2}{\tau_d} \quad (18)$$

where  $L$  is the thickness of the active layer that is equal to 100 nm in this study. The electron mobility  $\mu_n$  in the device can be calculated from the diffusivity  $D_n$  by using the following equation [40]:

$$\mu_n = \frac{q \times D_n}{kT}. \quad (19)$$

All the calculated results are presented in Table III. The charge mobility, as well as the diffusivity, is a curial parameter for the solar cell that can directly affect the fill factor. The high carrier

TABLE III  
ELECTRICAL PARAMETERS CALCULATED FROM THE FITTING OF THE NYQUIST PLOT BY USING THE EQUIVALENT CIRCUIT FOR BOTH FRESH AND AGED PBDB-T:ITIC-BASED DEVICES

| Parameters                               | PBDB-T:ITIC (Fresh)   | PBDB-T:ITIC (Aged)    |
|--|-----------------------|-----------------------|
| <b>τ<sub>d</sub> (μs)</b>                | 0.43                  | 2.06                  |
| <b>D<sub>n</sub> (cm<sup>2</sup>/s)</b>  | 2.30×10 <sup>-4</sup> | 4.84×10 <sup>-5</sup> |
| <b>μ<sub>n</sub> (cm<sup>2</sup>/Vs)</b> | 8.94×10 <sup>-3</sup> | 1.88×10 <sup>-3</sup> |

mobility indicates a high possibility for the carriers that can be collected [44], [45]. The diffusivity and electron mobility of the aged device all show a reduction, which correlates with the lower fill factor from the  $J$ - $V$  measurement.

As a method to investigate the recombination in the dark, the diode ideality factor  $n$  is extracted from the dark  $J$ - $V$  curve in Figs. 3(b) and S1(b) by using (3). Under the high voltage bias ( $>0.6$  V) for the PBDB-T:ITIC-based device and ( $>0.5$  V) for the PTB7:PC<sub>71</sub>BM and PffBT4T-2OD:PC<sub>71</sub>BM-based device in the exponential region, most of the current density to the voltage curve is influenced by the parasitic effects raised by shunt resistance and series resistance [21], [46]. Thus, corresponding to the dark current density to the voltage curve, the phenomenological differential diode ideality factors are calculated out at each voltage. The phenomenological differential ideality factor diagram for the PBDB-T:ITIC-based device is shown in Fig. 5. For the PTB7:PC<sub>71</sub>BM and PffBT4T-2OD:PC<sub>71</sub>BM-based device, the diagram is shown in Fig. S2(b). The tracing line indicates the minimum value of the diode ideality factor in the exponential region when the applied voltage is increasing. This minimum value is responsible for the reduced slope of dark  $J$ - $V$  curves due to the series resistance and shunt resistance [22]. Wolfgang *et al.* point out that when the minimum diode ideality factor value is very sharp in voltage, both series resistance and shunt resistance hardly allow to correctly determine the intrinsic diode ideality factor as the carrier recombination limited slope is not reached [22]. Therefore, the calculated minimum diode ideality factor can be considered as the upper limit for the phenomenological differential diode ideality factor. For the fresh PBDB-T:ITIC-based device, the value of the minimum diode ideality factor is found as 1.6054, while for the aged device, the value of the minimum diode ideality factor is found 1.8772. For the PTB7:PC<sub>71</sub>BM and PffBT4T-2OD:PC<sub>71</sub>BM-based device, the value of the minimum diode ideality factor is 1.790 and 1.664, respectively. It is worth to mention that the diode ideality factor is not related to the onset of the forward current in this case.

TABLE IV  
PARAMETERS RELATED TO THE DERIVED RELATION EQUATION AND CALCULATED CARRIER RECOMBINATION RESISTANCE

| Parameters   | PBDB-T:ITIC<br>(Fresh) | PBDB-T:ITIC<br>(Aged)  | PTB7:PC71BM            | PfFBT4T-<br>2OD:PC71BM |
|--|------------------------|------------------------|------------------------|------------------------|
| $n$  | 1.6054                 | 1.8772                 | 1.7906                 | 1.6436                 |
| $V_e$ (V)  | 0.82                   | 0.82                   | 0.55                   | 0.59                   |
| $J_{sc}$ (mA/cm <sup>2</sup> )   | 17.92                  | 17.50                  | 16.87                  | 17.60                  |
| $R_s$ ( $\Omega \cdot \text{cm}^2$ )   | 1.92                   | 1.62                   | 3.48                   | 2.53                   |
| $B = J_{sc}R_s$ (V)  | 0.0344                 | 0.0284                 | 0.0587                 | 0.0446                 |
| $q$ (J/eV)   | $1.6 \times 10^{-19}$  | $1.6 \times 10^{-19}$  | $1.6 \times 10^{-19}$  | $1.6 \times 10^{-19}$  |
| $K$ (J/K)  | $1.38 \times 10^{-23}$ | $1.38 \times 10^{-23}$ | $1.38 \times 10^{-23}$ | $1.38 \times 10^{-23}$ |
| $T$ (K)  | 298                    | 298                    | 298                    | 298                    |
| $R_{rec}$ ( $\Omega \cdot \text{cm}^2$ ) from<br>EIS   | 247.20                 | 172.80                 | 289.20                 | 951.60                 |
| $R_{rec}$ ( $\Omega \cdot \text{cm}^2$ )<br>calculated   | 241.02                 | 186.38                 | 287.95                 | 933.31                 |
| $\Delta R_{rec} = [R_{rec}(\text{calculated}) -$<br>$R_{rec}(\text{EIS})]/R_{rec}(\text{EIS})$ | 2.5%                   | 7.9%                   | 0.4%                   | 1.9%                   |

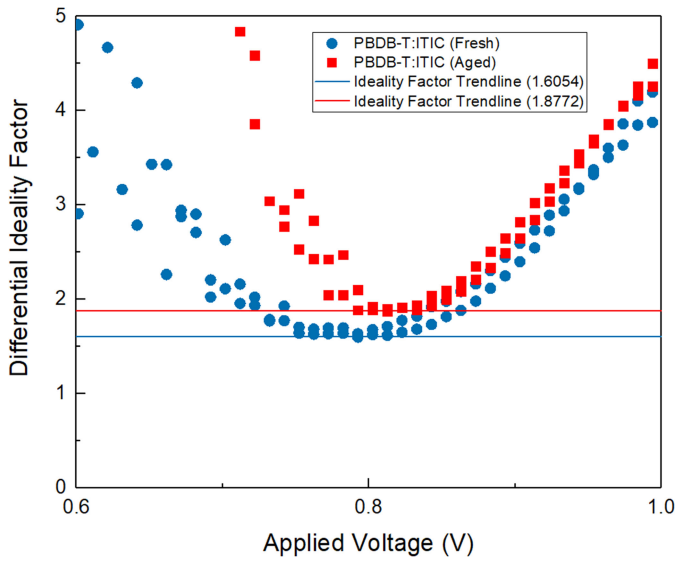


Fig. 5. Phenomenological differential ideality factor  $n$  calculated from the differential slope of the dark  $JV$  curve versus the voltage bias applied for fresh and aged PBDB-T:ITIC-based devices.

As the diode ideality factor from the dark  $J-V$  curve is known, the carrier recombination resistance can be calculated through a novel method by using the derived relation equation (16). The effective voltage  $V_e$  equals to the voltage that is used to extract the minimum diode ideality factor from a dark  $J-V$  curve, which makes the method consistent with the EIS study with effective measuring voltage. In this case, the value of  $V_e$  used for PBDB-T:ITIC, PTB7:PC<sub>71</sub>BM, and PfFBT4T-2OD:PC<sub>71</sub>BM-based device is around 0.82, 0.55, and 0.59 V, respectively. The voltage loss on series resistance component  $B$  is assumed to be equal to its maximum value  $J_{sc}R_s$  to minimize the effect of other ignored voltage losses. All the related parameters and the calculated carrier recombination resistance, as well as the carrier

recombination resistance extracted from the EIS, are displayed in Table IV.

In Table IV, it is easy to see that carrier recombination resistance calculated from the derived equation is comparable to the carrier recombination resistance extracted from EIS for all fabricated devices with less than 8% difference [ $\Delta R_{rec} = (R_{rec}(\text{calculated}) - R_{rec}(\text{EIS}))/R_{rec}(\text{EIS})$ ], which demonstrated the feasibility of the derived relation equation between the recombination resistance and the diode ideality factor. It is also easy to observe from the fresh and aged PBDB-T:ITIC-based devices that the recombination resistance and the diode ideality factor for the same type of device have a reverse relationship. The higher the carrier recombination resistance, the closer the value of the diode ideality factor approaching 1. The diode ideality factor equaling to unity ( $n = 1$ ) usually means that there is no trapping of charge carriers, and bimolecular recombination dominates the recombination in a device. With the diode ideality factor increasing, the trap-assisted recombination also grows in the space-charge region of photodevices [47]. The value of the diode ideality factor equaling to 2 predicts fully trap-assisted recombination in devices [48]. For bulk-heterojunction organic solar cells, the typically reported diode ideality factor value is in the range of 1.3–2.0, which is coherent with the results of this study [12], [49], [50]. The carrier recombination resistance is a parameter that is used to present the recombine process between holes and electrons [51]. It was found that the carrier recombination resistance is independent of electrodes, charge carrier generation ways and directly associated with the charge carrier recombination in the space-charge region of devices [52]. The carrier recombination resistance, as well as diode ideality factor estimation, is based on the dark condition in this study. These two factors obtained can more reasonably explain the nongeminate recombination of devices results from traps and defects. The high carrier recombination resistance indicates the higher resistivity to the nongeminate recombination, which also makes the

device to operate more closely to the ideal diode model. In nature, these two parameters aim to explain the same mechanism. Thus, deriving the relationship between the carrier recombination resistance and diode ideality factor is helpful to understand the nongeminate recombination of photodevices further.

#### IV. CONCLUSION

In this study, we have derived a novel relation equation to demonstrate the relationship between the carrier recombination resistance and the diode ideality factor of the photovoltaic device. To further illustrate this relationship, PBDB-T:ITIC-based nonfullerene organic solar cells and PTB7:PC<sub>71</sub>BM and PffBT4T-2OD:PC<sub>71</sub>BM-based fullerene organic solar cells were fabricated and a comparative study has been conducted between fresh devices and aged PBDB-T:ITIC-based devices. The aged PBDB-T:ITIC-based device exhibits degradation for all the electrical characteristics. The carrier recombination resistance in this study is extracted both by using the conventional method from the EIS and the derived relationship equation with the diode ideality factor extracted from dark  $J$ - $V$  curves. The results from these two different methods are comparable with less than 8% difference and the trends for the ideality factor versus the recombination resistance for the same type of device are also found. Thus, the validity of the relation equation between the ideality factor and recombination resistance is demonstrated. Moreover, the feasibility of a new method to extract the carrier recombination resistance is reported.

#### ACKNOWLEDGMENT

The authors would like to acknowledge the endless support from the staffs of Photovoltaic and Renewable Energy Engineering School, Electron Microscope Unit and Solid State and Elemental Analysis Unit under Mark Wainwright Analytical Centre, University of New South Wales.

#### REFERENCES

- [1] J. J. M. Halls *et al.*, "Efficient photodiodes from interpenetrating polymer networks," *Nature*, vol. 376, pp. 498–500, 1995.
- [2] J. Y. Kim *et al.*, "Efficient tandem polymer solar cells fabricated by all-solution processing," *Science*, vol. 317, no. 5835, pp. 222–225, 2007.
- [3] G. Yu, J. Gao, J. C. Hummelen, F. Wudl, and A. J. Heeger, "Polymer photovoltaic cells: Enhanced efficiencies via a network of internal donor-acceptor heterojunctions," *Science*, vol. 270, no. 5243, pp. 1789–1791, 1995.
- [4] H. Li, Z. Xiao, L. Ding, and J. Wang, "Thermostable single-junction organic solar cells with a power conversion efficiency of 14.62%," *Sci. Bull.*, vol. 63, no. 6, pp. 340–342, 2018.
- [5] Z. Xiao, X. Jia, and L. Ding, "Ternary organic solar cells offer 14% power conversion efficiency," *Sci. Bull.*, vol. 62, no. 23, pp. 1562–1564, 2017.
- [6] R. A. Street, A. Krakaris, and S. R. Cowan, "Recombination through different types of localized states in organic solar cells," *Adv. Funct. Mater.*, vol. 22, no. 21, pp. 4608–4619, 2012.
- [7] M. Andrea *et al.*, "Recombination dynamics as a key determinant of open circuit voltage in organic bulk heterojunction solar cells: A comparison of four different donor polymers," *Adv. Mater.*, vol. 22, no. 44, pp. 4987–4992, 2010.
- [8] R. C. I. MacKenzie, C. G. Shuttle, C. M. L. Chabiny, and J. Nelson, "Extracting microscopic device parameters from transient photocurrent measurements of P3HT:PCBM solar cells," *Adv. Energy Mater.*, vol. 2, no. 6, pp. 662–669, 2012.
- [9] C. G. Shuttle, R. Hamilton, B. C. O'Regan, J. Nelson, and J. R. Durrant, "Charge-density-based analysis of the current-voltage response of polythiophene/fullerene photovoltaic devices," *Proc. Nat. Acad. Sci. USA*, vol. 107, no. 38, pp. 16448–16452, 2010.
- [10] R. A. Street, "Localized state distribution and its effect on recombination in organic solar cells," *Phys. Rev. B*, vol. 84, no. 7, 2011, Art. no. 075208.
- [11] R. A. Street, S. Cowan, and A. J. Heeger, "Experimental test for geminate recombination applied to organic solar cells," *Phys. Rev. B*, vol. 82, no. 12, 2010, Art. no. 121301.
- [12] R. A. Street, M. Schoendorf, A. Roy, and J. H. Lee, "Interface state recombination in organic solar cells," *Phys. Rev. B*, vol. 81, no. 20, 2010, Art. no. 205307.
- [13] R. A. Street, K. W. Song, J. E. Northrup, and S. Cowan, "Photoconductivity measurements of the electronic structure of organic solar cells," *Phys. Rev. B*, vol. 83, no. 16, 2011, Art. no. 165207.
- [14] F. Alexander *et al.*, "Nongeminate recombination in planar and bulk heterojunction organic solar cells," *Adv. Energy Mater.*, vol. 2, no. 12, pp. 1483–1489, 2012.
- [15] A. Foertig, J. Rauh, V. Dyakonov, and C. Deibel, "Shockley equation parameters of P3HT:PCBM solar cells determined by transient techniques," *Phys. Rev. B*, vol. 86, no. 11, 2012, Art. no. 115302.
- [16] T. Kirchartz and J. Nelson, "Meaning of reaction orders in polymer:fullerene solar cells," *Phys. Rev. B*, vol. 86, no. 16, 2012, Art. no. 165201.
- [17] W. Tress, K. Leo, and M. Riede, "Dominating recombination mechanisms in organic solar cells based on ZnPC and C60," *Appl. Phys. Lett.*, vol. 102, no. 16, 2013, Art. no. 163901.
- [18] W. Shockley and W. T. Read, "Statistics of the recombinations of holes and electrons," *Phys. Rev.*, vol. 87, no. 5, pp. 835–842, 1952.
- [19] C. v. Berkel, M. J. Powell, A. R. Franklin, and I. D. French, "Quality factor in a-Si:H nip and pin diodes," *J. Appl. Phys.*, vol. 73, no. 10, pp. 5264–5268, 1993.
- [20] M. Bashahu and P. Nkundabakura, "Review and tests of methods for the determination of the solar cell junction ideality factors," *Sol. Energy*, vol. 81, no. 7, pp. 856–863, 2007.
- [21] T. Kirchartz, F. Deledalle, P. S. Tuladhar, J. R. Durrant, and J. Nelson, "On the differences between dark and light ideality factor in polymer:fullerene solar cells," *J. Phys. Chem. Lett.*, vol. 4, no. 14, pp. 2371–2376, 2013.
- [22] W. Tress *et al.*, "Interpretation and evolution of open-circuit voltage, recombination, ideality factor and subgap defect states during reversible light-soaking and irreversible degradation of perovskite solar cells," *Energy Environ. Sci.*, vol. 11, no. 1, pp. 151–165, 2018.
- [23] J. Bisquert *et al.*, "Doubling exponent models for the analysis of porous film electrodes by impedance. Relaxation of TiO<sub>2</sub> nanoporous in aqueous solution," *J. Phys. Chem. B*, vol. 104, no. 10, pp. 2287–2298, 2000.
- [24] V. Gonzalez-Pedro *et al.*, "General working principles of CH<sub>3</sub>NH<sub>3</sub>PbX<sub>3</sub> perovskite solar cells," *Nano Lett.*, vol. 14, no. 2, pp. 888–893, Feb. 2014.
- [25] J. R. Macdonald, "Impedance spectroscopy," *Ann. Biomed. Eng.*, vol. 20, no. 3, pp. 289–305, May 1992.
- [26] A. Lasia, "Electrochemical impedance spectroscopy and its applications," in *Modern Aspects of Electrochemistry*, B. E. Conway, J. O. M. Bockris, and R. E. White, Eds. Boston, MA, USA: Springer, 2002, pp. 143–248.
- [27] F. P. Gasparin, A. J. Bühler, G. A. Rampinelli, and A. Krenzinger, "Statistical analysis of I-V curve parameters from photovoltaic modules," *Sol. Energy*, vol. 131, pp. 30–38, 2016.
- [28] V. Gonzalez-Pedro *et al.*, "General working principles of CH<sub>3</sub>NH<sub>3</sub>PbX<sub>3</sub> perovskite solar cells," *Nano Lett.*, vol. 14, no. 2, pp. 888–893, 2014.
- [29] U. Würfel, D. Neher, A. Spies, and S. Albrecht, "Impact of charge transport on current-voltage characteristics and power-conversion efficiency of organic solar cells," *Nature Commun.*, vol. 6, 2015, Art. no. 6951.
- [30] M. A. Mahmud *et al.*, "Controlled nucleation assisted restricted volume solvent annealing for stable perovskite solar cells," *Sol. Energy Mater. Sol. Cells*, vol. 167, pp. 70–86, 2017.
- [31] D. Huang *et al.*, "Enhanced performance and morphological evolution of PTB7:PC<sub>71</sub>BM polymer solar cells by using solvent mixtures with different additives," *Phys. Chem. Chem. Phys.*, vol. 17, no. 12, pp. 8053–8060, 2015.
- [32] M. A. Mahmud *et al.*, "Simultaneous enhancement in stability and efficiency of low-temperature processed perovskite solar cells," *RSC Adv.*, vol. 6, no. 89, pp. 86108–86125, 2016.



- [33] J. D. Servaites, M. A. Ratner, and T. J. Marks, "Organic solar cells: A new look at traditional models," *Energy Environ. Sci.*, vol. 4, no. 11, pp. 4410–4422, 2011.
- [34] V. L. Dalal, R. Mayer, J. Bhattacharya, and M. Samiee, "Stability of organic solar cells," in *Proc 2012 IEEE Int. Rel. Phys. Symp.*, 2012, pp. 4A.5.1–4A.5.4.
- [35] T. Kirchartz *et al.*, "Sensitivity of the Mott–Schottky analysis in organic solar cells," *J. Phys. Chem. C*, vol. 116, no. 14, pp. 7672–7680, 2012.
- [36] J. Bisquert and G. Garcia-Belmonte, "On voltage, photovoltage, and photocurrent in bulk heterojunction organic solar cells," *J. Phys. Chem. Lett.*, vol. 2, no. 15, pp. 1950–1964, 2011.
- [37] G. Garcia-Belmonte, A. Guerrero, and J. Bisquert, "Elucidating operating modes of bulk-heterojunction solar cells from impedance spectroscopy analysis," *J. Phys. Chem. Lett.*, vol. 4, no. 6, pp. 877–886, 2013.
- [38] L. Burtone, D. Ray, K. Leo, and M. Riede, "Impedance model of trap states for characterization of organic semiconductor devices," *J. Appl. Phys.*, vol. 111, no. 6, 2012, Art. no. 064503.
- [39] B. Arredondo *et al.*, "Impedance spectroscopy analysis of small molecule solution processed organic solar cell," *Sol. Energy Mater. Sol. Cells*, vol. 128, pp. 351–356, 2014.
- [40] G. Garcia-Belmonte *et al.*, "Charge carrier mobility and lifetime of organic bulk heterojunctions analyzed by impedance spectroscopy," *Org. Electron.*, vol. 9, no. 5, pp. 847–851, 2008.
- [41] A. Aprilia *et al.*, "Influences of dopant concentration in sol–gel derived AZO layer on the performance of P3HT:PCBM based inverted solar cell," *Sol. Energy Mater. Sol. Cells*, vol. 111, pp. 181–188, 2013.
- [42] G. Perrier, R. de Bettignies, S. Berson, N. Lemaître, and S. Guillerez, "Impedance spectrometry of optimized standard and inverted P3HT-PCBM organic solar cells," *Sol. Energy Mater. Sol. Cells*, vol. 101, pp. 210–216, 2012.
- [43] B. Arredondo *et al.*, "Monitoring degradation mechanisms in PTB7:PC71BM photovoltaic cells by means of impedance spectroscopy," *Sol. Energy Mater. Sol. Cells*, vol. 144, pp. 422–428, 2016.
- [44] J. Bartelt, D. Lam, T. Burke, S. Sweetnam, and M. McGehee, "Charge-carrier mobility requirements for bulk heterojunction solar cells with high fill factor and external quantum efficiency >90%," *Adv. Energy Mater.*, vol. 5, no. 15, 2015, Art. no. 1500577.
- [45] B. Ebenhoch, S. A. J. Thomson, K. Genevičius, G. Juška, and I. D. W. Samuel, "Charge carrier mobility of the organic photovoltaic materials PTB7 and PC71BM and its influence on device performance," *Org. Electron.*, vol. 22, pp. 62–68, 2015.
- [46] G. A. H. Wetzelaer, M. Kuik, M. Lenes, and P. W. M. Blom, "Origin of the dark-current ideality factor in polymer:fullerene bulk heterojunction solar cells," *Appl. Phys. Lett.*, vol. 99, no. 15, 2011, Art. no. 153506.
- [47] C. T. Sah, R. N. Noyce, and W. Shockley, "Carrier generation and recombination in p-n junctions and p-n junction characteristics," *Proc. IRE*, vol. 45, no. 9, pp. 1228–1243, 1957.
- [48] R. N. Hall, "Electron-hole recombination in germanium," *Phys. Rev.*, vol. 87, no. 2, pp. 387–387, 1952.
- [49] T. Kirchartz, B. E. Pieters, J. Kirkpatrick, U. Rau, and J. Nelson, "Recombination via tail states in polythiophene:fullerene solar cells," *Phys. Rev. B*, vol. 83, no. 11, 2011, Art. no. 115209.
- [50] S. R. Cowan, L. W. Lin, B. Natalie, D. Gilles, and A. J. Heeger, "Identifying a threshold impurity level for organic solar cells: Enhanced first-order recombination via well-defined PC84BM traps in organic bulk heterojunction solar cells," *Adv. Funct. Mater.*, vol. 21, no. 16, pp. 3083–3092, 2011.
- [51] J. E. A. M. van den Meerakker, J. J. Kelly, and P. H. L. Notten, "The minority carrier recombination resistance: A useful concept in semiconductor electrochemistry," *J. Electrochem. Soc.*, vol. 132, no. 3, pp. 638–642, 1985.
- [52] S. R. Lunt, L. G. Casagrande, B. J. Tufts, and N. S. Lewis, "Studies of polycrystalline n-GaAs junctions: Effects of metal ion chemisorption on the photoelectrochemical properties of n-GaAs/KOH-Se/sup -/2-, n-GaAs/CH/sub 3/CH-ferrocene/sup +/0/, and n-GaAs/Au interfaces," *J. Phys. Chem.*, vol. 92, pp. 5766–5770, 1988.

Authors' photographs and biographies not available at the time of publication.